

# A segmented conical electric lens for optimization of the beam spot of the low-energy muon facility at PSI: a Geant4 simulation analysis

Ran Xiao<sup>a,b,c,\*\*</sup>, Elvezio Morenzoni<sup>c</sup>, Zaher Salman<sup>c</sup>, Bangjiao Ye<sup>a,b</sup>, Thomas Prokscha<sup>c,\*\*</sup>

<sup>a</sup>*State Key Laboratory of Particle Detection and Electronics, University of Science and Technology of China, Hefei 230026, P. R. China*

<sup>b</sup>*Department of Modern Physics, University of Science and Technology of China, Hefei 230026, P. R. China*

<sup>c</sup>*Laboratory for Muon Spin Spectroscopy, Paul Scherrer Institut, CH-5232 Villigen PSI, Switzerland*

---

## Abstract

The low energy muon (LEM) facility at PSI provides nearly fully polarized positive muons with tunable energies in the keV range to carry out muon spin rotation (LE- $\mu$ SR) experiments with nanometer depth resolution on thin films, heterostructures and near-surface regions. The low energy muon beam is focused and transported to the sample by electrostatic lenses. In order to achieve a minimum beam spot size at the sample position, and to enable the steering of the beam in horizontal and vertical direction, a special electrostatic device has been implemented close to the sample position. It consists of a cylinder at ground potential, followed by four conically shaped electrodes which can be operated at different electric potential. In LE- $\mu$ SR experiments an electric field at the sample along the beam direction can be applied to accelerate/decelerate muons to different energies (0.5-30 keV). Additionally, a horizontal or vertical magnetic field can be superimposed for transverse or longitudinal field  $\mu$ SR experiments. The focusing properties of the conical lens in the presence of these additional electric and magnetic fields have been investigated and optimized by

---

\*Corresponding author

\*\*Corresponding author

*Email addresses:* xran@mail.ustc.edu.cn (Ran Xiao), thomas.prokscha@psi.ch (Thomas Prokscha)

Geant4 simulations. Some experimental tests were also performed which show that the simulation well describes the experimental setup.

*Keywords:* muon beam, muon spin rotation, low energy, beam size, Geant4

---

## 1. Introduction

The muon spin rotation/relaxation/resonance ( $\mu$ SR) technique is a versatile local probe technique to investigate the physical properties of superconductors, magnetic systems, semiconductors and organic materials [1]. Polarized muon beams for  $\mu$ SR applications are usually produced at medium energy (0.5 - 3 GeV) proton accelerators. These muons have kinetic energies of the order of MeV and penetrate deeply into a sample (mm to cm). Therefore,  $\mu$ SR experiments using these MeV muons can only study bulk materials. To overcome these limitations and to extend  $\mu$ SR to the investigation of thin films, PSI developed and operates the low energy muons beam facility (LEM) where a cryogenic moderation method [2, 3, 4, 5, 6] is used to generate nearly fully polarized positive muons with tunable energies in the range of eV to several keV. Up to now the LEM facility at PSI has played a leading role in low energy muon experiments, extending the  $\mu$ SR technique to the investigation of nano-materials, layer interfaces, thin films and near-surface regions [7, 8, 9, 10, 11, 12, 13, 14, 15, 16, 17, 18, 19].

The LEM facility is located at the  $\mu$ E4 beam line, which is a hybrid-type large acceptance channel to generate an intense beam of so-called surface muons (positive muons,  $\mu^+$ , originating from pions decaying at rest close to the surface of the pion/muon target, with a kinetic energy of  $\sim 4$  MeV) [6]. The intensity of the surface muon beam at the exit of the  $\mu$ E4 beam line is about  $4.6 \times 10^8$ /s at a proton current of 2.2 mA. This represents at the moment the highest continuous surface muon flux in the world. About 40% of the beam is focused onto the cryogenic moderator target. Using a wide-band-gap van der Waals solid gas (s-N<sub>2</sub>, s-Ar) a moderation efficiency ( $\frac{N_{eV}^{out}}{N_{MeV}^{in}}$ ) between  $10^{-5}$  and  $10^{-4}$  is achieved [2, 4, 8].

The moderation of the muons from about 4 MeV to 10 eV is achieved within 10 ps, such that their initial high polarization is conserved [5]. The moderator consists of a 200-300 nm thick Ar layer (capped by a 10 nm thin N<sub>2</sub> layer) deposited on a thin Ag foil ( $\sim 125 \mu\text{m}$ ) [20] which is held by a cryostat at a temperature below 20 K. The mean energy of the moderated muons is about 15 eV with a width of about 20 eV (full width at half maximum, FWHM) [21]. These moderated muons can be re-accelerated by applying a high positive potential of up to 20 kV to the moderator [22]. After acceleration they are transported by electro- and magneto-static beam elements to the sample position. The rate of moderated muons at the sample is up to  $4.5 \times 10^3/\text{s}$ .

By tuning the high voltage of the moderator and the acceleration/deceleration high voltage at the sample, low-energy positive muons (LE- $\mu^+$ ) with tunable implantation energies between 0.5 and 30 keV are obtained, corresponding to mean implantation depths ranging from a few nm to a few hundred nm in solid materials [23]. In addition to the electric acceleration/deceleration field at the sample an external magnetic field – either parallel or perpendicular to the muon momentum – can be applied for transverse and longitudinal field  $\mu\text{SR}$  measurements. These fields may influence the beam spot size and position. A special optical element with four conically shaped segments (also called ring anode, RA) is used to focus the beam onto the sample. Its focusing and steering effects in combination with the applied electric and magnetic fields have been investigated using the musrSim simulation package [24] which is based on Geant4 [25, 26]. Using these simulations we optimize the settings of RA for the various magnetic fields and varying implantation energies (electric fields), and compare them with experimental data. These parameters allow to run the experiment with optimized beam transport onto the sample under different magnetic and electric field configurations. The results of this analysis are presented in this paper.

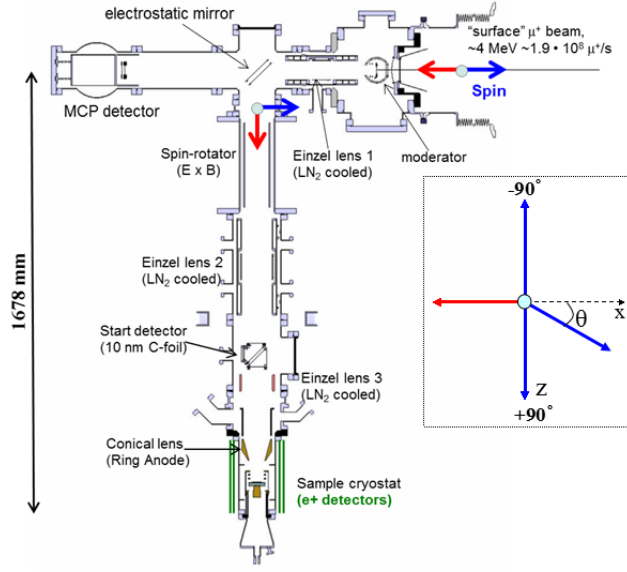


Figure 1: The layout of the low energy muon beam line for LE- $\mu$ SR experiments at PSI. The red and blue arrows in the figure represent the muon's momentum and direction of spin polarization, respectively.  $\theta_{spin}$  represents the spin angle with respect to the initial direction of the 4-MeV muon beam, corresponding to  $-x$  direction in the simulation.

## 2. Analysis of the effect of the external magnetic and electric fields at the sample position

## 3. Setup of the low energy muon beam

A schematic of the LEM apparatus is shown in Fig. 1. The low-energy muon beam is extracted from the cryogenic moderator with a quadratic area of  $30 \times 30 \text{ mm}^2$ . Adjustable positive high voltages applied to the moderator and to a set of grids generate an accelerating electric field to re-accelerate the moderated muons from eV to higher energies, typically between 10 keV and 20 keV (low energy muons). Only a small fraction of surface muons is moderated to eV energies, and most of the surface muons stop in the moderator target or leave the moderator with keV to hundreds of keV energies (fast muons). An electrostatic mirror with an angle of  $45^\circ$  with respect to the muon momentum is used to separate low energy from fast muons. After being focused by einzel lens 1 (L1) the low energy

muons are deflected by  $90^\circ$  with respect to the initial muon direction, while the fast ones continue in the direction of the MCP detector. After the deflection the spin polarization is perpendicular to the muon momentum. A spin rotator with

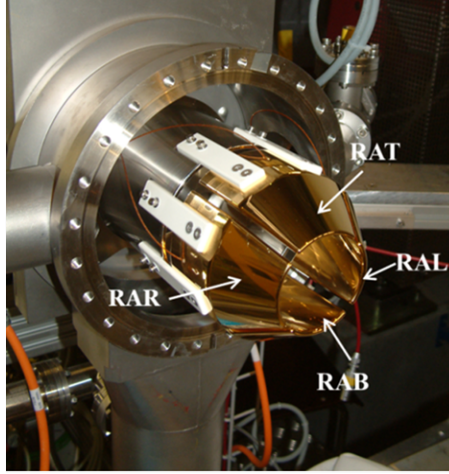


Figure 2: The four segments of the ring anode RA: the top segment RAT, the bottom segment RAB, the right segment RAR, and the left segment RAL, attached to a grounded stainless steel cylinder by pairs of macor insulators. The left and right segments of the RA sectors are named with respect to the muon beam direction.

crossed static magnetic and electric fields  $\vec{E} \times \vec{B}$  can be used to rotate the muon spin parallel or anti-parallel to its momentum [27]. This enables to carry out longitudinal field measurements (LF- $\mu$ SR, where the muon spin is parallel or anti-parallel to the applied field at the sample). The LE- $\mu^+$  spin angle ( $\theta_{spin}$ ) can be changed between  $-90^\circ$  to  $+90^\circ$  with respect to the initial direction of the 4-MeV muon beam by tuning the magnetic and electric fields in the spin rotator, such that the ratio E/B matches the velocity of the muons. Downstream of the spin rotator the einzel lens 2 (L2) focuses the muon beam onto the retractable start detector. This detector provides the fast start timing signal which is necessary for  $\mu$ SR experiments at a continuous muon beam. Its time resolution is about 1 ns, the detection efficiency for keV muons is  $\sim 80\%$ , and it introduces an increase of transverse phase space due to multiple scattering, and an increase of the initial width of the energy distribution of 20 eV FWHM to about 1 keV

FWHM. The detector is described in detail in Ref. [29, 30]. The final beam size at the sample position is determined by lens 3 (L3) and the strongly focusing conical lens RA. It consists of the four segments RAT, RAB, RAL and RAR, see Fig. 2. These segments are made of gold-plated, polished copper and are attached to a grounded stainless steel cylinder by pairs of macor or sapphire insulators. In contrast to an einzel lens the conical lens can be placed closer to the sample position, thus allowing for stronger focusing and a smaller beam spot. The beam can be shifted in horizontal and vertical direction by applying potential differences between the segments.

Compared to other low-energy particle beams with millimeter size beam extension and low emittances, the PSI low-energy muon beam has a large phase space due to the large source size of  $30 \times 30 \text{ mm}^2$ , the initial  $\cos \theta$  angular distribution (see Sec. 4), and the additional increase of phase space after passing the beam through the 10-nm-thin carbon foil of the start detector. This makes beam transport with a final small beam spot much more challenging.

#### **4. Optimization of RA focusing with applied external magnetic and electric fields at the sample**

In the LEM beam Geant4 simulation, the initial muon beam is started at the moderator, at the edge of the high-voltage acceleration region. The moderator is located at a distance of 499 mm upstream to the center of the electrostatic mirror. We assume homogeneous electric fields in the acceleration volume. In the simulation we studied the beam transport for various beam energies, i.e. moderator potentials  $V_{mod}$ : 10 kV, 12 kV, and 15 kV. The initial beam is homogeneously distributed on the moderator area of  $30 \times 30 \text{ mm}^2$ , and the initial mean kinetic energy is 15 eV with a FWHM of 20 eV. Due to the homogeneous angular distribution of slow muons inside the moderator [20] a  $\cos \theta$  angular distribution is generated in the simulation for muons escaping from the moderator layer, where  $\theta$  is the angle of the muon momentum with respect to the initial beam direction (the  $-x$  direction in the simulation).

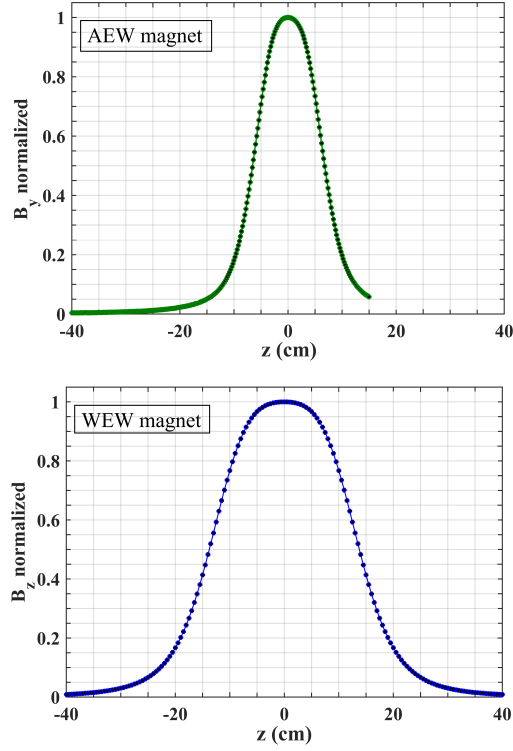


Figure 3: Normalized magnetic field along beam axis  $z$  of the AEW magnet (measured) and WEW magnet (calculated).  $z = 0$  corresponds to the sample position.

Field maps of the beam elements (Spin Rotator, L1, L2, L3 and RA) have been either calculated or measured [27, 28, 30], and are scaled according to the experimental settings. In the electrostatic mirror a homogeneous electric field is assumed.

A vertical magnetic field up to 300 Gauss, parallel to the sample surface, is supplied by the AEW magnet for transverse field  $\mu$ SR measurements (TF- $\mu$ SR, muon spin transverse to the applied field), and a magnetic field of up to 3400 Gauss can be applied perpendicular to the sample surface and along the muon beam direction (WEW magnet, LF- or TF- $\mu$ SR, depending on the initial muons spin polarization). The AEW magnet consists of air-cooled coils (8 A maximum current) wound around a soft-iron yoke with a magnet gap of 154 mm. Because

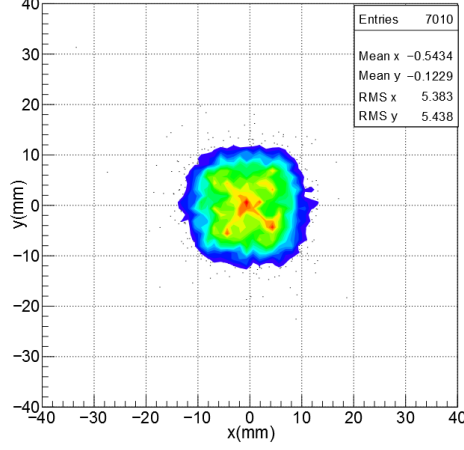


Figure 4: The simulated beam spot without external fields at the sample position using optimized experimental high voltage settings for the beam line elements at  $V_{mod}=15$  kV,  $\theta_{spin}=-10^\circ$ : L1=9.0 kV, L2=10.5 kV, L3=11.5 kV and RA=11.9 kV. The initial number of muons at the moderator ( $N^{in}$ ) is  $10^4$ .

of this large gap, soft-iron pieces inside the vacuum tube are used to reduce the effective length of the magnet and its fringe field region, and to increase the maximum available magnetic field at the sample position. The WEW magnet consists of two water-cooled coils, made of square copper-hollow conductors (600 A maximum current), in Helmholtz geometry, surrounded by a soft-iron housing to reduce the stray fields outside of the magnet, and to maximize the available field at the sample position. The iron housing of the magnet has a length of 285 mm in beam direction, and a front face size of  $540 \times 540$  mm<sup>2</sup>. The magnetic field along the beam axis is shown for both magnets in Fig. 3. The effective lengths of the magnets are 152 mm for the AEW magnet, and 295 mm for the WEW magnet.

An acceleration/deceleration high voltage of up to  $\pm 12.5$  kV can be applied at the sample plate in order to tune the final implantation energy of the LE- $\mu^+$ .



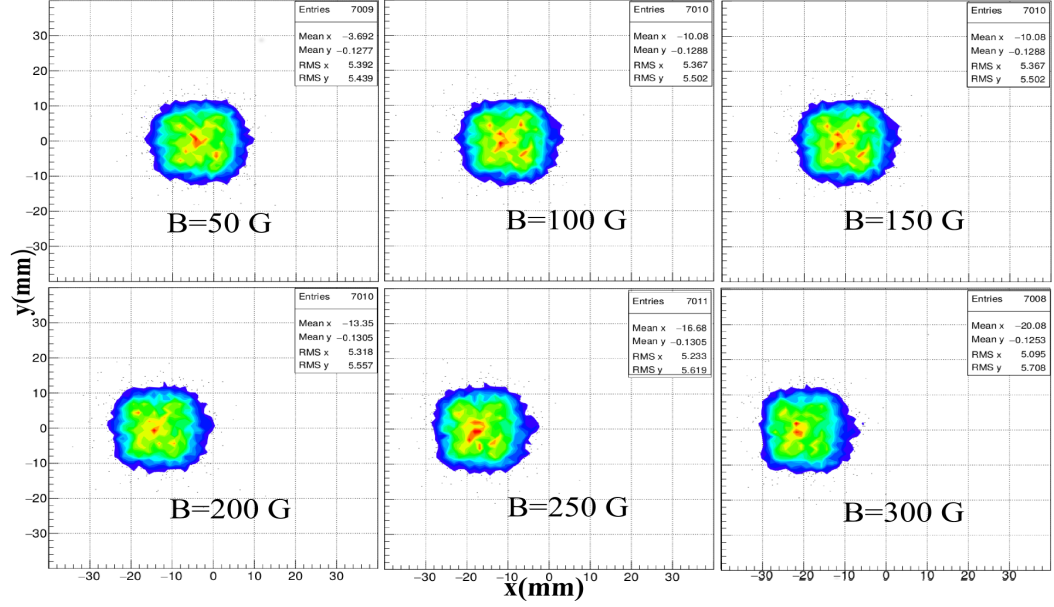


Figure 5: Simulated beam spots at the sample viewed from downstream in different AEW magnetic fields (50 to 300 Gauss) with the same beam element settings as in Fig. 2.

#### 4.1. Beam spot with vertical magnetic field

##### 4.1.1. Effect of vertical magnetic field on beam spot

In this section we investigate the effects of the vertical magnetic field (AEW magnet) and of an accelerating/decelerating electric field at the sample on the beam spot for different fields and implantation energies. In addition, we simulate the steering and focusing effects of RA. This allows us to optimize the RA settings for the different magnetic field configurations, which can be used as reference values for the experiment. Figure 4 shows the simulated muon beam spot at the sample position for a muon extraction voltage of  $V_{mod} = 15$  kV without external fields at the sample. The beam spot is well centered in this case, in agreement with the experiment (not shown). Figure 5 shows beam spots without electric field at the sample, viewed from downstream for different AEW magnetic fields: 50, 100, 150, 200, 250 and 300 Gauss. The beam spot shifts almost linearly to the left with increasing magnetic field while the shape of

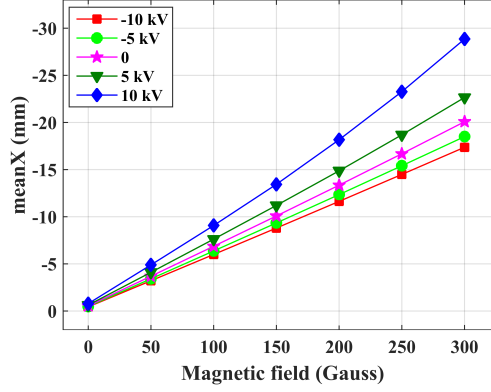


Figure 6: meanX values with electric potentials at the sample from -10 kV to 10 kV and AEW magnetic fields from 0 to 300 Gauss ( $V_{mod} = 15$  kV)

the beam spot is only marginally affected. The mean vertical position remains almost constant. The mean horizontal position (meanX) for different electric fields and vertical magnetic fields are shown in Fig. 6. The absolute value of meanX increases nearly linearly with increasing magnetic field, and the beam spot shift is larger in a decelerating electric field. In order to keep the beam spot in the center a potential difference has to be applied between the RAL and RAR segments of RA. Its effect on the beam spot is studied in the next subsection.

#### 4.1.2. Effect of beam steering by RA

The effect of beam steering by applying a potential difference between opposite RA segments is illustrated in Fig. 7 for beam transport with  $V_{mod} = 10$  kV, where we compare the experimental and simulated beam spots at the sample. In the experiment, the beam spot at the sample position is measured using a 44 mm diameter Roentdek DLD40 delay line detector with three resistance matched Hamamatsu MCPs in a Z configuration. The top two beam spots of Fig. 7 are for RAL-RAR = -0.64 kV (RAL = 7.18 kV, RAR = 7.82 kV, RAT = RAB = 7.50 kV), where the beam spot center shifts to the left side with meanX = -9.5 mm (in experiment) and -8.4 mm (in simulation). The results

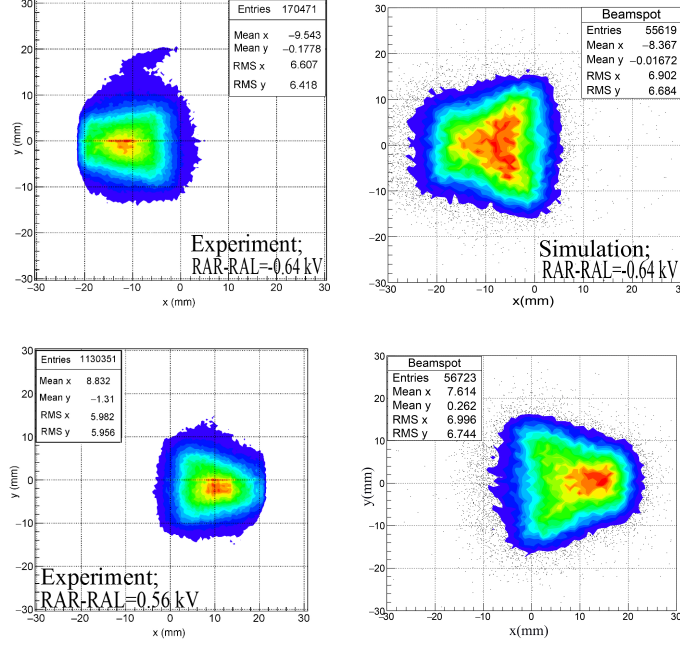


Figure 7: Comparison of measured and simulated beam spots at the sample viewed from upstream with  $RAT = RAB$ , and  $RAL-RAR = -0.64$  kV (top), and  $0.56$  kV (bottom). Other parameters are :  $V_{mod}=10.0$  kV,  $L1= 6.0$  kV,  $L2=7.0$  kV,  $L3=8.0$  kV,  $RAT=RAB=7.5$  kV,  $\theta_{spin} = -10^\circ$ . The initial number of muons at the moderator in the simulation is  $10^5$ .

for  $RAL-RAR = 0.56$  kV ( $RAL = 7.78$  kV,  $RAR = 7.22$  kV,  $RAT = RAB = 7.50$  kV) are shown in the bottom two figures. In this case the beam spot shifts to the right side with  $meanX = 8.8$  mm (in experiment) and  $7.6$  mm (in simulation). The agreement between experiment and simulation is fairly good. The small deviations can be explained by the uncertainty in the applied potentials in the experiment. The used high voltage power supplies have an absolute uncertainty between  $10$  V and  $30$  V, which results in an overall uncertainty of about  $50$  V per power supply by taking into account additional uncertainties in the analog control of the power supplies. The beam spot is deformed to a trapezoidal shape, which is different from the effect of the magnetic field which doesn't cause a deformation. This deformation is caused by lens aberrations in the RA due to proximity of the beam to the electrodes and the broken four fold

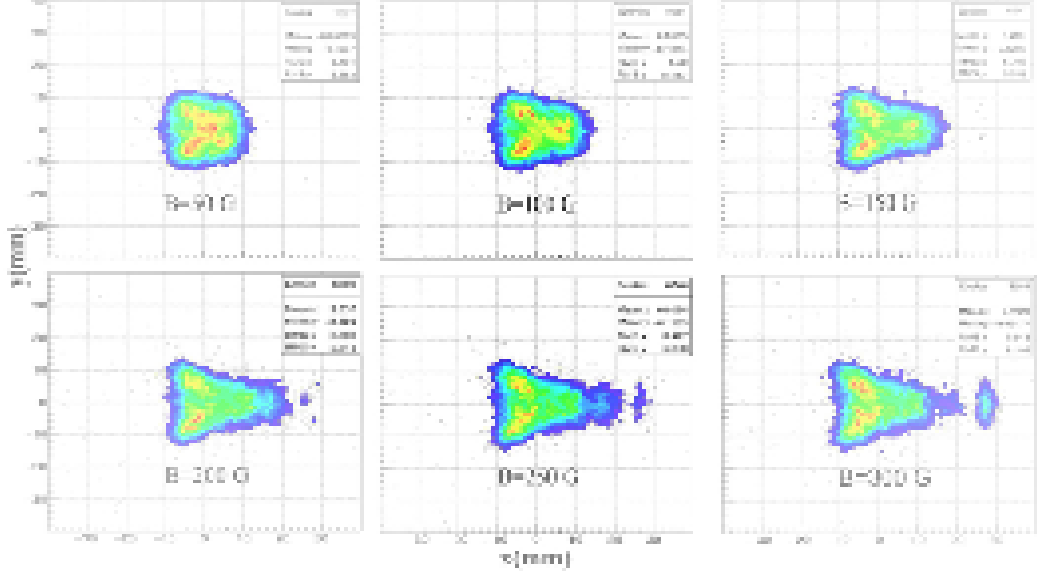


Figure 8: Simulated beam spots at the sample position viewed from downstream with maximized number of muons in the center. The centering of the beam spot is obtained by using the RA potential differences given in Tab. 1. Vertical magnetic field (AEW magnet) varies from 50 Gauss to 300 Gauss with the same beam element settings as in Fig. 4 ( $V_{mod}=15$  kV,  $RA=11.9$  kV). Pictures from left to right, top to bottom are the beam spots with different AEW magnetic fields (50 to 300 Gauss) at the sample with zero sample bias.

symmetry of the electric field in case of a potential difference applied between two opposite segments. In the simulation, the transmission from the moderator to the sample at 10 kV is about 55%, compared to about 70% at 15 kV, where we define the transmission as  $\frac{N^{out}}{N^{in}} \times 100\%$ , with  $N^{out}$  the number of muons in the sample plane, and  $N^{in}$  the initial number of muons at the moderator. The reduction of the transmission is due to i) a longer time-of-flight at 10 kV, which increases the fraction of muons decaying in flight by about 5% at 10 kV compared to 15 kV, ii) a 10% higher muonium formation (bound neutral state of a  $\mu^+$  and an  $e^-$ ) probability in the 10-nm-thin carbon foil of the start detector, and iii) larger beam divergence at 10 kV after the start detector. In the experiment we observe a corresponding drop of event rate when changing the

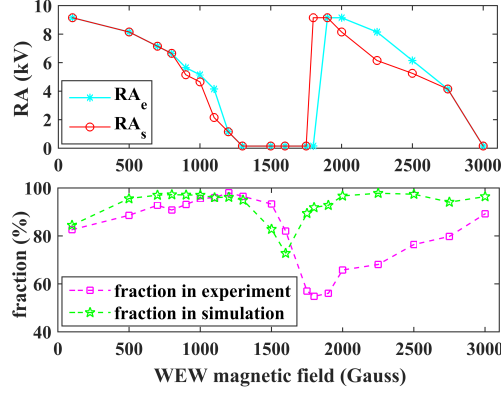


Figure 9: Optimized RA potential values (top) and the corresponding fractions (bottom) of the beam stopping in the central area of  $20 \times 20 \text{ mm}^2$  at the sample for different WEW magnetic fields for a moderator potential of 12 kV.  $RA_e$  and  $RA_s$  are the best values in the experiments and simulations, respectively.

beam transport settings from 15 kV to 10 kV.

Table 1: Simulated optimum values of (RAL-RAR) (Unit: kV) to steer the beam spot to the center at different electric potentials at the sample between -10 kV and 10 kV, and different AEW magnetic fields from 0 to 300 Gauss,  $V_{mod}=15 \text{ kV}$ .  $RAL+RAR=23.8 \text{ kV}$ .

	-10 kV	-5 kV	0	5 kV	10 kV
50 G	-0.36	-0.38	-0.40	-0.50	-0.6
100 G	-0.68	-0.70	-0.76	-0.82	-0.9
150 G	-1.00	-1.10	-1.20	-1.20	-1.2
200 G	-1.25	-1.50	-1.70	-1.60	-1.6
250 G	-1.60	-1.70	-1.85	-2.00	-2.0
300 G	-2.00	-2.10	-2.20	-2.30	-2.4

#### 4.1.3. Centering of the beam spot at the sample by RA steering

A potential difference between the RAL and RAR segments allows to counteract the action of the AEW magnetic field and to steer the beam spot back to the center at the sample position. For muons extracted with 15 kV at the moderator and whose beam spot shifts are shown in Fig. 5, the optimum potential

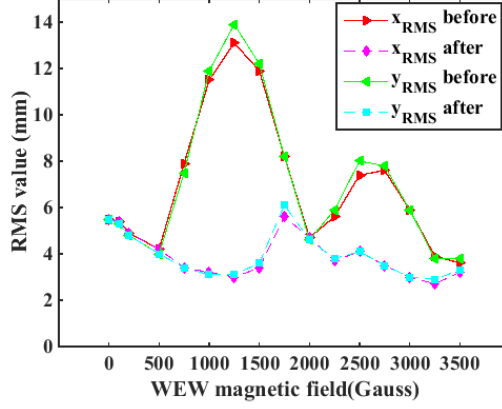


Figure 10:  $x_{RMS}$  and  $y_{RMS}$  of the muon beam spot at the sample at different WEW magnetic fields before and after tuning RA with  $V_{mod}=15$  kV. Data labeled "before" and "after" are for RA=11.9 kV for all magnetic fields before optimizing RA in the simulation and after setting the RA according to the values of Tab. 3, respectively.

differences obtained by the simulation are shown in Tab. 1 for different sample potentials (i.e. implantation energies) and AEW magnetic fields. The other transport element parameters in the simulation are the same as those given in Fig. 4.

Figure 8 shows the simulated beam spots after centering by using the RA parameters given in Tab. 1. The shape of the beam spot is deformed with increasing  $|RAL-RAR|$  to a trapezoid instead of the initial square. When  $|RAL-RAR| > 2$  kV the beam spot splits into two parts, the larger one keeping the previous trapezoidal shape, and the smaller one having an ellipsoidal shape. This splitting causes the meanX value to deviate from zero, while the muon rate in the center of the sample plane is maximized.

The fraction  $\eta = N_{[-10,10]mm}^{out}/N^{out}$  of muons stopping in an area of  $x, y \in [-10, 10]$  mm in the center of the beam spot is shown in Tab. 2 after RA steering. Before adjusting RA this fraction is smaller than 10% when a 300-Gauss magnetic field is applied, and it further reduces to less than 1% when a positive bias of +5 kV and +10 kV is applied at the sample. After steering, most of the muons ( $> 60\%$ ) are shifted to the  $20 \times 20$  mm<sup>2</sup> area in the center.

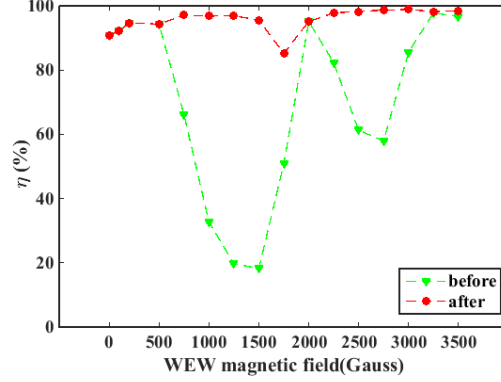


Figure 11: The fraction  $\eta$  of muons stopping in the central area of  $20 \times 20 \text{ mm}^2$  at the sample position with different WEW magnetic fields parallel to the muon before and after optimizing RA with  $V_{mod}=15 \text{ kV}$ . Data labeled "before" and "after" are for RA=11.9 kV for all magnetic fields (before optimizing RA in the simulation) and after tuning RA according to Tab. 3, respectively.

#### 4.2. Beam spot with horizontal magnetic field

In this section we investigate the effects of a horizontal magnetic field parallel to the beam axis on the beam spot for different fields and implantation energies. This magnetic field at the sample is generated by the WEW magnet for LF- and TF- $\mu$ SR experiments. The muon beam spot at the sample may be influenced by the WEW magnetic field by field components perpendicular to the muon momentum. An experimental determination of the optimal RA settings is obtained by maximizing the fraction  $\eta$  of muons landing within an area of  $20 \times 20 \text{ mm}^2$  at the sample position. This can be done by measuring the TF- $\mu$ SR precession amplitude on a  $20 \times 20 \text{ mm}^2$  gold foil glued onto a Ni coated large plate. Muons stopping in the gold foil maintain their polarization and hence contribute to the measured signal, while muons landing in the Ni backing depolarize almost immediately and do not contribute to the precession amplitude. Measurements of the precession amplitude as a function of RA voltage were performed using the positron detectors, with  $V_{mod} = 12 \text{ kV}$ . Figure 9 shows good agreement between experimental ( $RA_e$ ) and simulated ( $RA_s$ ) optimum RA values for WEW fields up to 1600 Gauss. At higher fields there are

Table 2: The fraction  $\eta$  of muons stopping in an area of  $20 \times 20 \text{ mm}^2$  in the center of the beam spot after steering by RA according to Tab. 1 for different electric and AEW magnetic fields,  $V_{mod}=15 \text{ kV}$ . (Unit:%)

	-10 kV	-5 kV	0 kV	5 kV	10 kV
0	93.7	93.2	91.9	90.4	87.6
50 G	93.3	92.7	91.7	89.0	86.2
100 G	91.7	91.3	88.8	86.2	81.1
150 G	88.6	85.4	81.4	73.2	64.3
200 G	84.0	85.0	74.1	69.4	63.2
250 G	80.5	79.6	76.9	66.4	56.5
300 G	79.4	75.2	68.9	62.4	62.1

Table 3: Optimized RA potential values for different WEW magnetic fields,  $V_{mod}=15 \text{ kV}$ .

B/Gauss	100	200	500	750	1000	1250	1500	1750	2000	2250	2500	2750	3000	3250
RA/kV	11.9	11.9	11.9	10.0	7.6	3.8	0	0	11.2	10.5	7.2	4.2	0.0	0.0

differences up to about 2500 Gauss, where the  $RA_s$  values deviate by one to two kV from the experimental  $RA_e$  optimum settings. At even higher fields  $RA_e$  and  $RA_s$  agree again up to the maximum measured field of 3000 Gauss. We attribute the discrepancies to a slightly off-centered beam in the experiment and possible differences between the calculated WEW field map used in the simulation and the actual experimental one. The off-centered beam is caused by a slightly tilted muon moderator target and possible misalignment of optical elements, which in turn introduces additional transverse velocity components in the beam, causing a shift and off-centered beam spot as a function of magnetic field. This affects the fraction of muons stopping in the central area of  $20 \times 20 \text{ mm}^2$ .

The RMS values of simulated beam spots at different WEW magnetic field from 0-3500 Gauss at  $V_{mod}=15 \text{ kV}$  are displayed in Fig. 10. For RA fixed at



11.9 kV the beam size significantly increases between 500 Gauss and about 2000 Gauss due to the varying focusing power of the magnet. This can be corrected by lowering the RA potential to reduce the focusing power of RA. As in the case of the  $V_{mod} = 12$  kV data the RA potential was tuned to maximize the fraction  $\eta$  of muons stopping in the central area of  $20 \times 20$  mm<sup>2</sup> of the sample plane. Table 3 summarizes these optimized RA potential values to achieve the smallest beam spot size at the sample. One can see that the RA voltage can be kept constant up to 500 Gauss before it has to be lowered to compensate for the increasing focusing power of the magnet. At some magnetic fields (such as  $B=1500, 1700$  Gauss) there is no need to use the RA to focus the beam ( $RA=0$ ). Compared to the  $V_{mod} = 12$  kV data the RA has to be turned on again to obtain the smallest beam spot at a field of about 2000 G, which is higher than the  $\sim 1750$  G at  $V_{mod} = 12$  kV. This shift is expected due to the  $\sqrt{15 \text{ keV}/12 \text{ keV}}$  higher momentum of the muon beam: at higher beam momentum one needs a correspondingly higher magnetic field to obtain the same beam transport properties of the WEW magnetic field. Figure 11 compares the fraction  $\eta$  at the sample before and after tuning the RA at different WEW magnetic fields. It is obvious that  $\eta$  can be significantly increased by proper tuning of RA. The fractions  $\eta$  at  $V_{mod} = 15$  kV are higher than at  $V_{mod} = 12$  kV because of the smaller increase of transverse phase space when passing through the carbon foil of the start detector: the mean scattering angle due to multiple scattering is lower at higher beam energy.

## 5. Summary

In this paper we presented the focusing and steering properties of a segmented conical electrostatic lens (RA) which serves as a lens with large focusing power for the keV muon beam of the LE- $\mu^+$  facility at PSI. This beam optics element is essential for obtaining a small beam spot in the very limited space available in the sample region of the LE- $\mu$ SR setup. We presented a detailed Geant4 investigation of the beam transport to optimize the experimental con-

ditions for the present LEM setup, where we studied the beam transport onto the sample plane in the presence of various magnetic and electric fields in the sample region. In some cases the availability of experimental data allowed comparing the simulation with the experimental data. Good agreement is found, which demonstrates that the optical properties of RA are well described in the simulation. Using the simulation we optimized the electric potential settings of RA in the case of a vertical magnetic field at the sample position. This field is transverse to the muon momentum and requires steering by RA to center the beam spot. In the case of a magnetic field along the beam direction the increasing focusing power of the magnet has to be compensated by a reduction of the RA focusing power. The simulation can be used to optimize RA for various experimental conditions in the sample region without the need of running an experiment to test the beam properties at the sample position for each case. This is important for the design and analysis of future LE- $\mu$ SR experiments. A long term goal is the reduction of the beam spot size to allow the investigation of standard  $5 \times 5 \text{ mm}^2$  samples. At present, the study of such samples is only possible by using a mosaic of at least four pieces of this size. In many cases it is not possible to generate four or more identical samples, which makes some experiments unfeasible. To achieve this long term goal the understanding and the reliability of the simulation of the used optical beam elements is essential, especially the design of the last focusing element where the present work provides important information. Finally, we emphasize that Geant4 simulations are very powerful to describe and optimize experimental setups and to help pushing experimental capabilities to the limit.

## 6. Acknowledgements

Ran Xiao acknowledges a scholarship from the China Scholarship Council (CSC) and financial support from PSI for her stay at PSI.

## References

- [1] Yaouanc A, de Réotier P D, Muon Spin Rotation, Relaxation, and Resonance: Applications to Condensed Matter, Oxford University Press, 2011, 14–29.
- [2] Morenzoni E, Physics and applications of low energy muons, Muon Science: Muons in Physics, Chemistry and Materials (Bristol and Philadelphia, 1999), SL Lee, SH Kilcoyne, and R. Cywinski, Eds, 1998, **51**: 343–404.
- [3] Morenzoni E, Glückler H, Prokscha T, *et al.* Low-energy  $\mu$ SR at PSI: present and future, Physica B: Condensed Matter, 2000, **289**: 653–657. DOI:10.1016/S0921-4526(00)00303-3
- [4] Harshman D, Mills Jr A, Beveridge J, *et al.* Generation of slow positive muons from solid rare-gas moderators, Phys Rev B, 1987, **36**: 8850. DOI:10.1103/PhysRevB.36.8850
- [5] Morenzoni E, Kottmann F, Maden D, *et al.* Generation of very slow polarized positive muons, Phys Rev Lett, 1994, **72**: 2793. DOI:10.1103/PhysRevLett.72.2793
- [6] Prokscha T, Morenzoni E, Deiters K, *et al.* The new  $\mu$ e4 beam at PSI: A hybrid-type large acceptance channel for the generation of a high intensity surface-muon beam, Nucl Instrum Methods A, 2008, **595**: 317–331. DOI:10.1016/j.nima.2008.07.081
- [7] Morenzoni E, Khasanov R, Luetkens H, *et al.* Low energy muons as probes of thin films and near surface regions, Physica B: Condensed Matter, 2003, **326**:196–204. DOI:10.1016/S0921-4526(02)01601-0
- [8] Morenzoni E, Prokscha T, Suter A, *et al.* Nano-scale thin film investigations with slow polarized muons, J Phys: Cond Matter, 2004, **16**: S4583. DOI:10.1088/0953-8984/16/40/010

- [9] Prokscha T, Chow K, Stilp E, *et al.* Photo-induced persistent inversion of germanium in a 200-nm-deep surface region, *Sci Rep*, 2013,**3**: 2569 DOI:10.1038/srep02569
- [10] Morenzoni E, Prokscha T, Saadaoui H, *et al.* Low-energy muons at PSI: Examples of investigations of superconducting properties in near-surface regions and heterostructures, in: *Proceedings of the International Symposium on Science Explored by Ultra Slow Muon (USM2013)*, JPS Conference Proceedings, Vol. 2, id. 010201, 10 pp., Vol. 2, 2014, p. 0201. DOI:10.7566/JPSCP.2.010201
- [11] Schulz L, Nuccio L, Willis M, *et al.* Engineering spin propagation across a hybrid organic/inorganic interface using a polar layer, *Nature Mater*, 2011,**10**: 39–44. DOI:10.1038/nmat2912
- [12] Suter A, Morenzoni E, Prokscha T, *et al.* Two-dimensional magnetic and superconducting phases in metal-insulator  $\text{La}_{2-x}\text{Sr}_x\text{CuO}_4$  superlattices measured by muon-spin rotation, *Phys Rev Lett*, 2011,**106**:237003. DOI:10.1103/PhysRevLett.106.237003
- [13] Boris A, Y. Matiks Y, Benckiser E, *et al.* Dimensionality control of electronic phase transitions in nickel-oxide superlattices, *Science*, 2011,**332**: 937–940. DOI:10.1126/science.1202647
- [14] Hofmann A, Salman Z, Mannini M, *et al.* Depth-dependent spin dynamics in thin films of  $\text{TbPc}_2$  nanomagnets explored by low-energy implanted muons, *ACS Nano*, 2012, **6**: 8390–8396. DOI:10.1021/nn3031673
- [15] Stilp E, Suter A, Prokscha T, *et al.* Controlling the near-surface superfluid density in underdoped  $\text{YBa}_2\text{Cu}_3\text{O}_{6+x}$  by photo-illumination, *Sci Rep*, 2014, **4**:6250. DOI:10.1038/srep06250
- [16] Saadaoui H, Salman Z, Luetkens H, *et al.* The phase diagram of electron-doped  $\text{La}_{2-x}\text{Ce}_x\text{CuO}_{4-\delta}$ , *Nat Commun*, 2015, **6**: 6041. DOI: 10.1038/ncomms7041

- [17] Al MaMari F, Moorsom T, Teobaldi G, *et al.* Beating the stoner criterion using molecular interfaces, *Nature*, 2015, **524**: 69–73. DOI:10.1038/nature14621
- [18] Anghinolfi L, Luetkens H, Perron J, *et al.* Thermodynamic phase transitions in a frustrated magnetic metamaterial, *Nat Commun*, 2015, **6**: 8278. DOI:10.1038/ncomms9278
- [19] Flokstra M, Satchell N, Kim J, *et al.* Remotely induced magnetism in a normal metal using a superconducting spin-valve, *Nature Physics*, 2016, **12**: 57–61. DOI:10.1038/nphys3486
- [20] Prokscha T, Morenzoni E, David C, *et al.* Moderator gratings for the generation of epithermal positive muons, *Appl Surf Sci*, 2001, **172**: 235–244. DOI:10.1016/S0169-4332(00)00857-6
- [21] Bakule P, Morenzoni E, Generation and applications of slow polarized muons, *Contemporary Physics*, 2004, **45**: 203–225. DOI:10.1080/00107510410001676803
- [22] Low energy muons: Overview of the experimental setup, <http://www.psi.ch/low-energy-muons/experimental-setup>.
- [23] Morenzoni E, Glückler H, Prokscha T, *et al.* Implantation studies of keV positive muons in thin metallic layers, *Nucl Instrum Methods B*, 2002, **192**: 254–266. DOI:10.1016/S0168-583X(01)01166-1
- [24] Sedlak K, Scheuermann R, Shiroka T, *et al.* musrSim and musrSimAna-simulation tools for  $\mu$ SR instruments, *Physics Procedia*, 2012, **30**: 61–64. DOI:10.1016/j.phpro.2012.04.040
- [25] Agostinelli S, Allison J, Amako K, *et al.* Geant4a simulation toolkit, *Nucl Instrum Methods A*, 2003, **506**: 250–303. DOI:10.1016/S0168-9002(03)01368-8

- [26] Allison J, Amako K, Apostolakis J, *et al.* Geant4 developments and applications, Nuclear Science, 2006, **53**: 270–278. DOI:10.1109/TNS.2006.869826
- [27] Salman Z, Prokscha T, Keller P, *et al.* Design and simulation of a spin rotator for longitudinal field measurements in the low energy muons spectrometer, Physics Procedia, 2012, **30**: 55–60. DOI:10.1016/j.phpro.2012.04.039
- [28] Paraiso T K, Morenzoni E, Prokscha T, *et al.* Geant4 simulation of low energy  $\mu$ SR experiments at PSI, Physica B: Condensed Matter, 2006, **374**: 498–501. DOI:10.1016/j.physb.2005.11.140
- [29] Morenzoni E, Birke M, Glückler H, *et al.* Generation of very slow polarized muons by moderation, Hyperfine Interactions, 1997, **106**: 229–235. DOI:10.1023/A:1012610528798
- [30] Khaw K S, Antognini A, Crivelli P, *et al.* Geant4 simulation of the PSI LEM beam line: energy loss and muonium formation in thin foils and the impact of unmoderated muons on the  $\mu$ SR spectrometer, Journal of Instrumentation, 2015, **10**: 10025. DOI:10.1088/1748-0221/10/10/P10025